Mon. Not. R. Astron. Soc. **000**, ??–?? (2012) Printed 4 March 2013 (MN LaTeX style file v2.2)

arXiv:1205.4939v1 [astro-ph.HE] 22 May 2012

The radio structure of ultra-high-energy synchrotron peak BL Lacs

Zhongzu Wu[1]*, D. R. Jiang[2], Minfeng Gu[2]

[1] *College of Science, Guizhou University, Guiyang 550025, China.*
[2] *Key Laboratory for Research in Galaxies and Cosmology, Shanghai Astronomical Observatory, Chinese Academy of Sciences, 80 Nandan Road, Shanghai 200030, China*

4 March 2013

ABSTRACT

We present the results of EVN and MERLIN 5 GHz observations of nine ultra-high-energy synchrotron peak BL Lacs (UHBLs) selected as all BL Lacs with **log** ($\nu_{\rm peak}$/Hz) > 20 from Nieppola et al.. The radio structure was investigated for these sources, in combination with the available VLBA archive data. We found that the core-jet structure is detected in five sources, while four sources only have a compact core on pc scale. The core of all sources shows high brightness temperature (with mean and median values **log** ($T_{\rm b}$/K) ~ 11 , which implies that the beaming effect likely present in all sources. When the multi-epoch VLBI data are available, we found no significant variations either for core or total flux density in two sources (2E 0414+0057 and EXO 0706.1+5913), and no evident proper motion in 2E 0414+0057, while the superluminal motion is likely detected in EXO 0706.1+5913. Our sources are found to be less compact than the typical HBLs in Giroletti et al, by comparing the ratio of the VLBI total flux to the core flux at arcsec scale. Combining all our results, we propose that the beaming effect might be present in the jets of UHBLs, however, it is likely weaker than that of typical HBLs. Moreover, we found that UHBLs could be less Doppler beamed versions of HBLs with similar jet power, by comparing the distribution of redshift, and radio luminosities. The results are in good consistence with the expectations from our previous work.

Key words: BL Lac objects – galaxies: active – quasars: general

1 INTRODUCTION

BL Lac objects are a type of radio loud active galactic nuclei (AGNs) with no emission lines or less of them and characterized by the nonthermal radiation over the entire electromagnetic spectrum. They can be classified as different subclasses based on their spectral energy distribution (SED), namely, low frequency peaked BL Lac objects (LBL), intermediate objects (IBL) and high frequency peaked BL Lac objects (HBL) (Padovani & Giommi 1995). Generally, LBLs are intrinsically more luminous than HBLs with the 5 GHz radio luminosity, γ-ray luminosity and the luminosity at peak frequency $\nu_{\rm peak}$ of the synchrotron component, which is called blazar sequence (see Fossati et al. 1998; Ghisellini et al. 1998, for details).

The power - $\nu_{\rm peak}$ anti-correlation suggested by blazar sequence has been tested by larger blazar samples in recent years; however, the results are controversial (Padovani 2007). Meyer et al. (2011) shows that blazar sequence is formed from two populations in the synchrotron $\nu_{\rm peak}$ - $L_{\rm peak}$ plane, each forming an upper edge to an envelope of progressively misaligned blazars and most intermediate synchrotron peak (ISP) sources are not intermediate in intrinsic jet power between LSP and high synchrotron-peaking (HSP) sources, but are more misaligned versions of HSP sources with similar jet powers. Rani et al. (2011) found that the changes in the jet Doppler factor is the most important one among the model parameters responsible for changes in the observed SEDs of blazars. Wu et al. (2007) found a significant anti-correlation between the intrinsic $\nu_{\rm peak}$ and the total luminosity at 408 MHz, which is less affected by the beaming effect thus represents the intrinsic radio emission. As a whole, LBLs are found to be more powerful than HBLs. The authors claimed that HBLs have smaller Doppler factor and larger viewing angle than LBLs. Intriguingly, after eliminating the beaming effect in both parameters,

---

* E-mail: zzwu08@gmail.com

Nieppola et al. (2008) and Wu et al. (2009) found a positive correlation between the synchrotron peak frequency and luminosity, which is opposite to the blazar sequence.

In order to understand the differences between the subclasses of BL Lacs, the high resolution radio observations have been performed to explore the jet properties for HBLs and LBLs, and the comparison between these two populations were made. The VLBI observations showed that most LBLs display superluminal motions (Chen et al. 1999; Gabuzda et al. 2000; Jorstad et al. 2001), while the TeV blazars (most are HBLs) display subluminal or mildly relativistic motions (Giroletti et al. 2004b, 2006; Piner & Edwards 2004). Rector et al. (2003) observed 15 HBLs and 3 RGB BL Lacs, and found that HBLs, like most LBLs, show parsec-scale core-jet morphologies with complex kilo-parsec scale morphologies. Moreover, the jets in HBLs are more well aligned, suggesting that their jets are either intrinsically straighter or are seen further off-axis than LBLs. Giroletti et al. (2004a) selected 30 low redshift BL Lac objects and confirmed that HBLs show less distortion and therefore, are expected to be oriented at larger angles than LBLs. All these findings seem to be consistent with the results of Wu et al. (2007), of which HBLs have larger viewing angles than that of LBLs.

Ghisellini et al. (1999) suggested that there is a class of BL Lacs with the synchrotron peak at higher frequencies than that of conventional HBLs, i.e. $\mathbf{log}$ $(\nu_{\rm peak}/{\rm Hz}) > 19$, and these sources can be called ultra-high-energy synchrotron peak BL Lacs (UHBLs) (Giommi et al. 2001). As these sources are at the extreme end of $\nu_{\rm peak}$ distribution, the investigation of radio compact structure, and jet property are thus crucial in studying BL Lacs populations. As Wu et al. (2007) suggested, UHBLs are expected to have smaller Doppler factor, larger viewing angle, and lower radio luminosity. However, as far as we know, the VLBI observations are only presented for a few UHBLs, and the radio compact structures of UHBLs are largely unknown. In this paper, we investigate the radio structure of UHBLs based on our EVN and MERLIN observations and VLBI archive data.

The layout of this paper is as follows. In Section 2, the observations and data reduction are presented. The results are described in Section 3. The discussions are shown in Section 4, while the conclusions are drawn in Section 5. Throughout the paper, we define the spectral index α as $f_\nu \propto \nu^{-\alpha}$, where f_ν is the flux density at frequency ν, and a cosmology with $H_0 = 70$ km s^{-1} Mpc^{-1}, $\Omega_{\rm M} = 0.3$, $\Omega_\Lambda = 0.7$ is adopted.

2 OBSERVATION AND DATA REDUCTION

Nieppola et al. (2006) have constructed the SEDs for a large, heterogeneous sample of BL Lacs taken from the Veron-Cetty & Veron BL Lac catalogue and visible from the Metshähovi radio observatory. This is the first time the SEDs of BL Lacs have been studied with a sample of over 300 objects. In the sample, 22 BL Lacs with $\nu_{\rm peak} > 10^{19}$ Hz were classified as UHBLs candidates. From these sources, we selected all nine sources with $\mathbf{log}$ $(\nu_{\rm peak}/{\rm Hz}) > 20$, which represent the extreme population of UHBLs. In order to explore their radio structure, the VLBI simultaneous observations with EVN and MERLIN, were carried out at 5 GHz for these sources in February 2009 with a total observing time of 24 hours. The phase reference technique was used for all sources except for 2E 0414+0057 and EXO 0706.1+5913. The phase calibrators were found in the VLBA calibrators, whose distances from the targets are less than 3 degrees. In order to get higher angular resolution, we request also two Chinese telescopes, but unfortunately, the Urumqi station was unavailable during the observation. The recording rate of 1 Gb/s was adopted, and the scan time around 1.5 hours was taken for each source.

Besides our observations, we also collected the available VLBA archive data. All these observations are listed in Table 1. The data reduction were performed using the NRAO Astronomical Image Processing System (AIPS). The imaging and model fitting were carried out with DIFMAP package (Shepherd, Pearson & Taylor 1994). The image parameters for our EVN and MERLIN observations are listed in Table 2: Col. (1) source name, Col. (2) redshift, Cols. (3) - (4) the observational date and the half-power beamwidth (HPBW) of the weighted beam, Col. (5) the noise of the image, Col. (6) the peak flux of the image, Col. (7) VLBI array.

3 RESULTS

The radio components from the circular gaussian model fitting for EVN images are listed in Table 3, in which Col. (1) is the source name, Col. (2) the observation epoch, Col. (3) the observation frequency, Col. (4) the label of radio components, Col. (5) the flux density and uncertainties of corresponding components (in mJy), Col. (6) the distance of component to core (in mas), Col. (7) the position angle of component, Col. (8) the radius of components, and Col. (9) the brightness temperature (see Section 4.1). All the uncertainties of the component parameters were derived using the formula given by Andrei Lobanov [1].

3.1 Source position

With the phase-reference technique, we are able to obtain the accurate positions from the VLBI data, which are listed in Table 4 for seven sources. All the celestial positions we used for correlation are from NASA/IPAC Extragalactic Database (NED)[2]. Our results show that the accurate position for RXS J1341+3959 and RXS J1410+6100 are significantly different from the positions provided by NED, with position difference larger than $10''$. The accurate positions for these two sources can only be derived from our MERLIN data (see Table 4), which however, are much closer to that from the Faint Images of the Radio Sky at Twenty Centimeters (FIRST) 1.4-GHz radio catalogue (Becker, White & Helfand 1995), with a position difference less than $0''.3$ and $0''.5$, respectively. The accurate positions of other sources are obtained from the EVN data, which might be more accurate than those from the FIRST images.

---

[1] http://www.radionet-eu.org/rda/archive/eris-11_lobanov.pdf

[2] http://ned.ipac.caltech.edu/

Table 1. The VLBI observation log.

Object	z	Epoch (years)	Freq (GHz)	Array
2E 0414+0057	0.287	1996.68	4.99	VLBA
		1997.38	4.99	VLBA
		1999.70	4.99	VLBA
		2004.73	4.99	VLBA
		2004.73	8.42	VLBA
		2009.16	4.99	EVN+MERLIN
		2010.99	8.65	VLBA
		2011.02	8.65	VLBA
EXO 0706.1+5913	0.125	2002.13	5.00	VLBA
		2004.73	4.99	VLBA
		2004.73	8.42	VLBA
		2009.16	4.99	EVN+MERLIN
		2010.93	8.65	VLBA
1ES 0927+500	0.14	2009.16	4.99	EVN+MERLIN
		2010.15	8.42	VLBA
		2010.15	15.37	VLBA
RXS J1012.7+4229	0.364	2009.16	4.99	EVN+MERLIN
RGB 1319+140	0.573	2009.16	4.99	EVN+MERLIN
RXS J1341+3959	0.163	2009.16	4.99	EVN+MERLIN
		2009.79	8.42	VLBA
		2009.79	15.37	VLBA
RXS J1410+6100	0.384	2009.16	4.99	EVN+MERLIN
RXS J1458.4+4832	0.541	2009.16	4.99	EVN+MERLIN
RXS J2304.6+3705	0.57	2009.16	4.99	EVN+MERLIN

Table 2. The EVN+MERLIN image parameters.

Object	z	HPBW (mas × mas,°)	Noise (3σ) (mJy beam^{-1})	Peak (mJy beam^{-1})	Array
1ES 0927+500	0.14	2.63×1.61, 22.2	0.18	12.4	1
		63.3×41.2, -62.8	1.06	23.7	2
		2.75×1.69, 22.8	0.17	12.6	1+2
RXS J1012.7+4229	0.364	4.7×2.49, -3.4	0.15	19.6	1
		62.4×42.3, 43.1	1.04	32.6	2
		4.9×3.62, -9.27	0.31	19.9	1+2
RGB 1319+140	0.573	6.23×2.1, 15.2	0.263	26.2	1
		70.4×49.7, 23.5	1.4	41.7	2
		6.35×2.23, 15.6	0.302	32.2	1+2
RXS J1341+3959	0.163	5.82×2.23, 30.7	0.25	6.9	1
		54.4×46.6, 41	0.979	22.0	2
RXS J1410+6100	0.384	2.79×2.07, 2.23	0.17	7.15	1
		53.9×48.1, -79.8	0.81	17.6	2
RXS J1458.4+4832	0.541	4.19×2.28, 30.2	0.168	7.7	1
		52.6×46.5, 29.9	0.844	18.4	2
RXS J2304.6+3705	0.57	4.89×2.19, 0.999	0.092	9.72	1
		63.6×40.6, 47.5	1.12	22.2	2

1: EVN, 2: MERLIN.

3.2 Individual sources

3.2.1 2E 0414+0057

The radio structure has been studied by Rector et al. (2003) and Kharb et al. (2008). The 5 GHz VLA image of this source shows a jet like feature at P.A. ∼ 40°, while the VLBI images show a jet in P.A. ∼ 75° (Kharb et al. 2008). The VLBA map resolves a jet that initially extends to the east-northeast (P.A. ∼ 68°) of the core and also weak, extended (∼ 3 - 4 σ) emission to the southeast of the jet, which suggests either that the jet is collimated and bends to the south ∼ 10 pc from the core, or that the projected jet opening angle is wide (∼ 60°). The inner portion of the jet is well aligned (ΔP.A. = 5°) to the kpc-scale jet (Rector et al. 2003).

The radio structure of our EVN and MERLIN observation for this source is shown in Fig. 1, as well as one VLBA image as comparison. There are two jet components in VLBA image, however, one of them is absent in our EVN

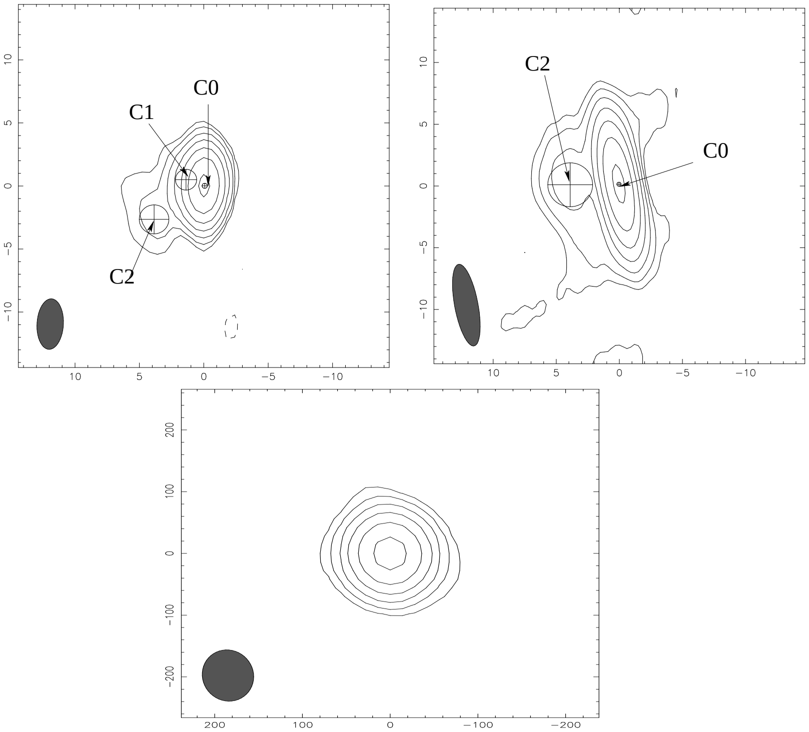

Figure 1. The radio structure of 2E 0414+0057: upper left - VLBA at 5 GHz, epoch 1997.38; upper right - our EVN observation; bottom: Our MERLIN observation. The core, and two jet components are labeled with C0, C1 and C2, respectively. The contour levels are (-1, 1, 2, 4, 8, 16, 32, 64) multiples the 3σ level. The horizontal axis is the relative R. A., and the vertical axis is the relative Dec. to the source position in mas.

image, while the MERLIN image shows only a compact core. All the measured parameters for core and jet components are listed in Table 3, from which it can be seen that the P.A. of inner jet component ranges from 56° to 90°, while it is 88° - 124° for the outer one. Therefore, our results also suggest that the jet of this source has a wide opening angle. Based on the multi-epoch VLBI data, we calculated the spectrum index of core with average flux at 4.9 and 8.6 GHz, and found it is with $\alpha = 0.26$.

3.2.2 EXO 0706.1+5913

The 1.4 GHz VLA image shows that the radio core is located on the north-west edge of a roughly spherical cocoon. It was suggested that this object could be a wide-angle or narrow-angle tailed object, viewed at a small angle. The 5 GHz VLBA image shows a weak jet to the south-west (Giroletti et al. 2004a).

We present our EVN and MERLIN image of this source in Fig. 2. The core and three jet components are detected from EVN observation, and their parameters are listed in Table 3 for all the VLBI data. We found that the P.A. of jet components from all the VLBI data ranges from -128° to -170°, indicating that the projected jet opening angle is likely around 42°. A flat spectra is found with α=0.22 for the core, using the average flux at 4.9 and 8.6 GHz from multi-epoch VLBI data (see Table 3).

3.2.3 1ES 0927+500

This source was observed with VLA config A at 1.4 GHz, with a peak flux density 19.9 mJy and no information is available on the pc-scale morphology (Giroletti et al. 2004a). Our EVN, MERLIN and EVN+MERLIN images (Fig. 3) shows that this source has a compact core, and the weak diffuse emission at south-east to the core is detected at EVN and EVN+MERLIN images. The measured core parameters are shown in Table 3.

3.2.4 RXS J1012.7+4229

The total flux at 1.4 GHz for this source is around 79 mJy from both FIRST and the NRAO VLA Sky Survey (NVSS) . Our EVN, MERLIN and EVN+MERLIN images are shown in Fig. 4. The EVN, EVN+MERLIN images show that there is a jet bending to the northeast direction. Consistently, there is a hint of jet structure towards the northeast direction in the MERLIN image. Two jet components are found with P.A. around 6° and 25°, respectively, which is shown in Table 3.

3.2.5 RXS J1319+1405

The total flux at 1.4 GHz for this source is around 65.8 mJy from FIRST catalogue. Our EVN and MERLIN images are presented in Fig. 5. The EVN and EVN+MERLIN images of this source shows a core-jet structure with jet towards east

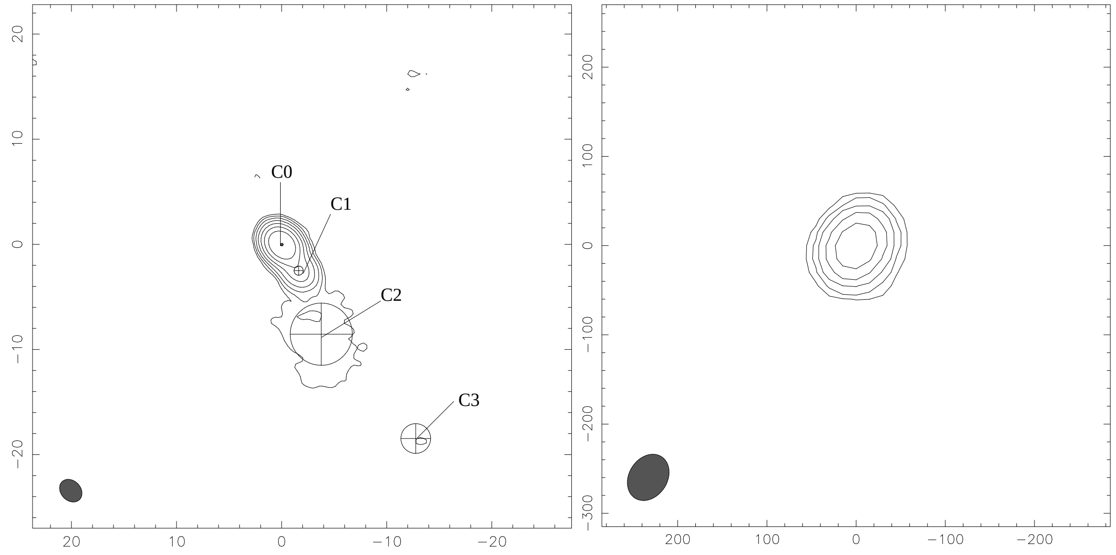

Figure 2. The radio structure of EXO 0706.1+5913 from our EVN and MERLIN observation: left - our EVN observation; right our MERLIN observation. The core and three jet components are marked in the image. The contour levels are (1, 2, 4, 8, 16, 32, 64) multiples the 3σ level. The horizontal axis is the relative R. A., and the vertical axis is the relative Dec. to the source position in mas.

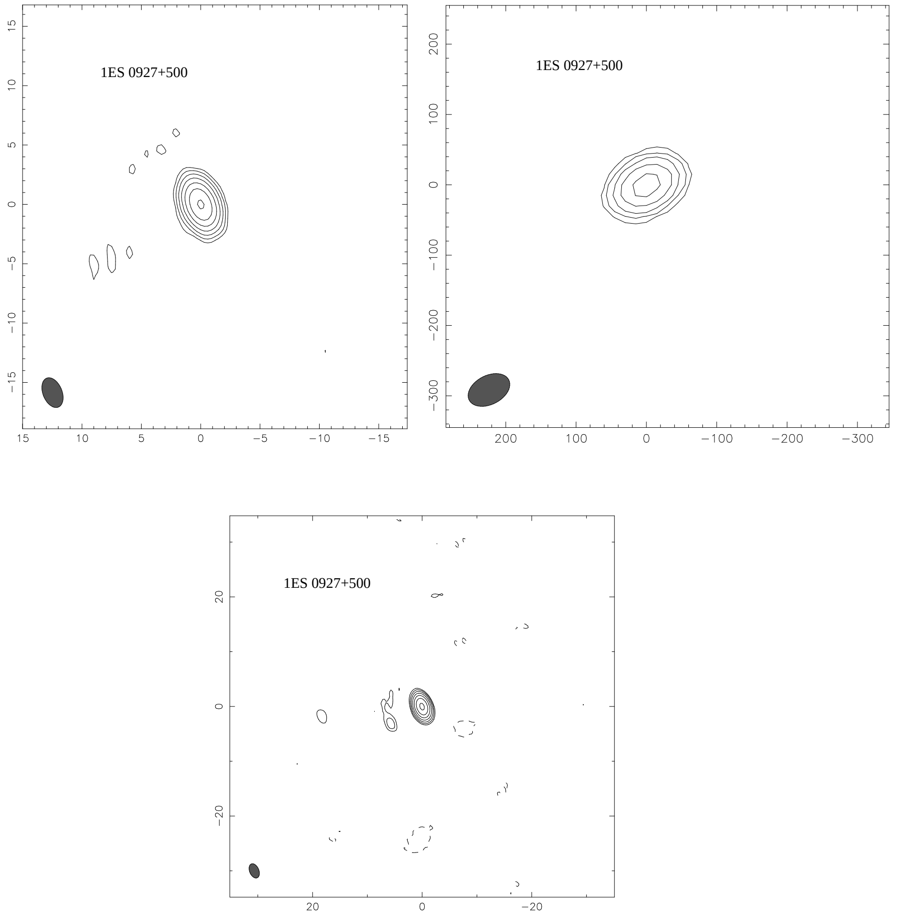

Figure 3. The EVN (upper left), MERLIN (upper right) and EVN+MERLIN (bottom) images of 1ES 0927+500 at 5 GHz. The contour levels are (-1, 1, 2, 4, 8, 16, 32, 64...) multiples the minimum contour level, which is 3 times the rms noise given in Table 2. The horizontal axis is the relative R. A., and the vertical axis is the relative Dec. to the source position in mas.

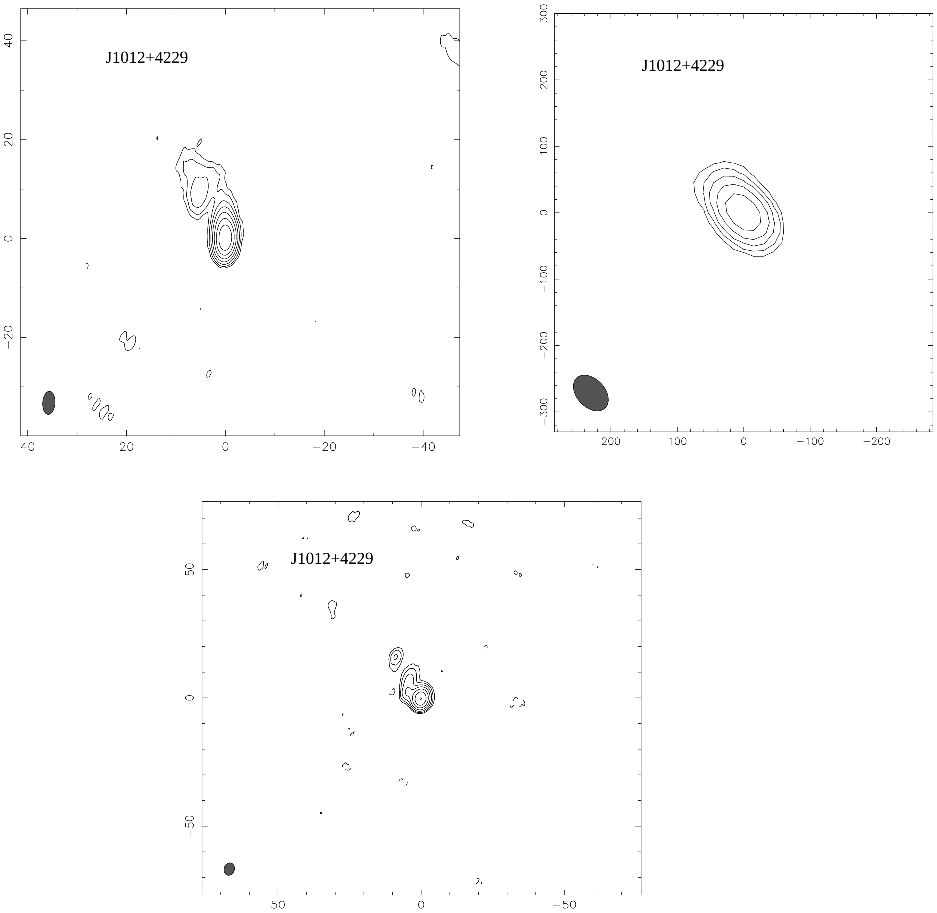

Figure 4. The EVN (upper left), MERLIN (upper right) and EVN+MERLIN (bottom) images of RXS J1012.7+4229 at 5 GHz. The contour levels are (-1, 1, 2, 4, 8, 16, 32, 64...) multiples the minimum contour level, which is 3 times the rms noise given in Table 2. The horizontal axis is the relative R. A., and the vertical axis is the relative Dec. to the source position in mas.

direction with P.A. around 80° (see Table 3). In the MERLIN image, the sign of weak emission is found at much larger distance, but at similar direction. The image parameters are shown in Table 2.

3.2.6 RXS J1341+3959

The total flux at FIRST 1.4 GHz for this source is around 39.9 mJy. Both the EVN and MERLIN images show a compact core, which is presented in Fig. 6. The image parameters are shown in Table 2.

3.2.7 RXS J1410+6100

The total flux at 1.4 GHz for this source is around 5.4 mJy from VLA FIRST. Similar to RXS J1341+3959, a compact core is observed from both the EVN and MERLIN images (Fig. 7), with the image parameters shown in Table 2. We found that the EVN 5 GHz core flux density is about 7.2 mJy, which however is higher than the FIRST VLA 1.4 GHz total flux. This indicates that either the radio spectrum is invert, or there is variations in the flux at these two radio bands.

3.2.8 RXS J1458.4+4832

The total flux at 1.4 GHz for this source is around 2.5 mJy from VLA NVSS. We show our radio images in Fig. 8. The EVN image shows a compact core, while MERLIN image shows weak diffuse emission at a large scale towards northeast direction. Similar to RXS J1410+6100, the EVN 5 GHz total flux ∼7.6 mJy and the MERLIN peak flux ∼18.4 mJy/beam are apparently larger than the total NVSS flux, which implies either a invert spectrum or flux variation in RXS J1458.4+4832.

3.2.9 RXS J2304.6+3705

The total flux at 1.4 GHz for this source is around 22.5 mJy from VLA NVSS data. Our EVN image shows a possible jet structure towards northwest direction with P.A. $\sim -60^\circ$ (see Fig. 9 and Table 3). It has a total radio flux around 11 mJy from EVN image. The MERLIN image shows only a compact core, with peak flux about 22 mJy/beam.

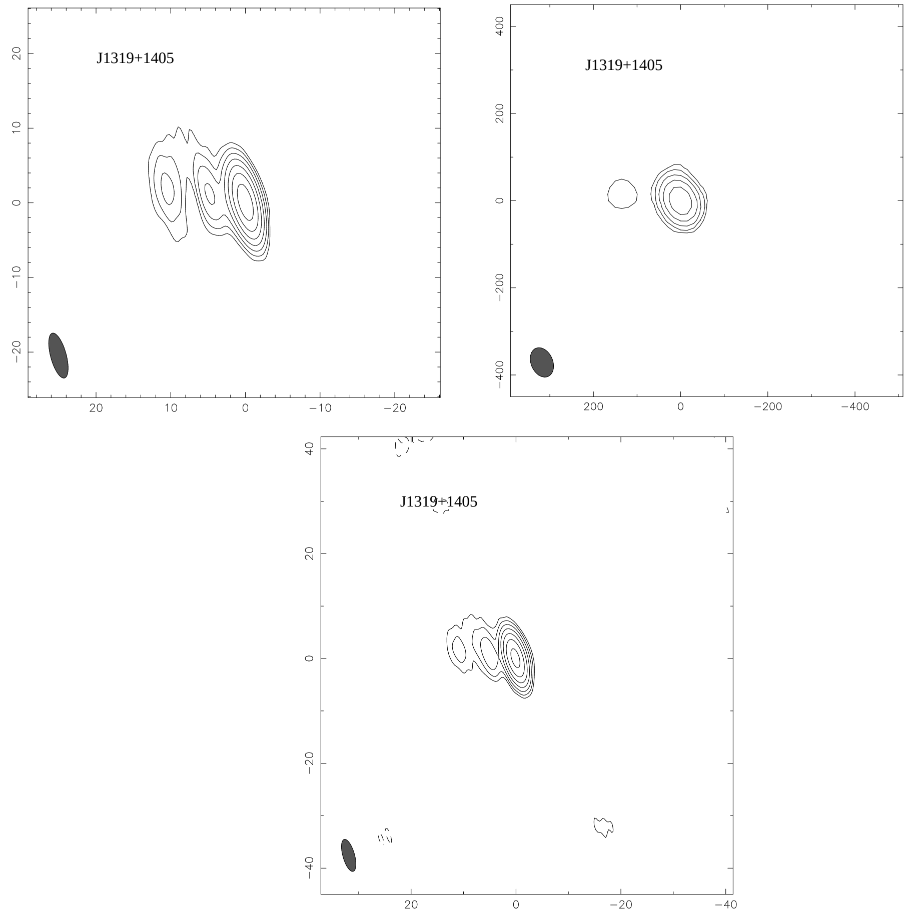

Figure 5. The EVN (upper left), MERLIN (upper right) and EVN+MERLIN (bottom) images of RXS J1319+1405 at 5 GHz. The contour levels are (-1, 1, 2, 4, 8, 16, 32, 64...) multiples the minimum contour level, which is 3 times the rms noise given in Table 2. The horizontal axis is the relative R. A., and the vertical axis is the relative Dec. to the source position in mas.

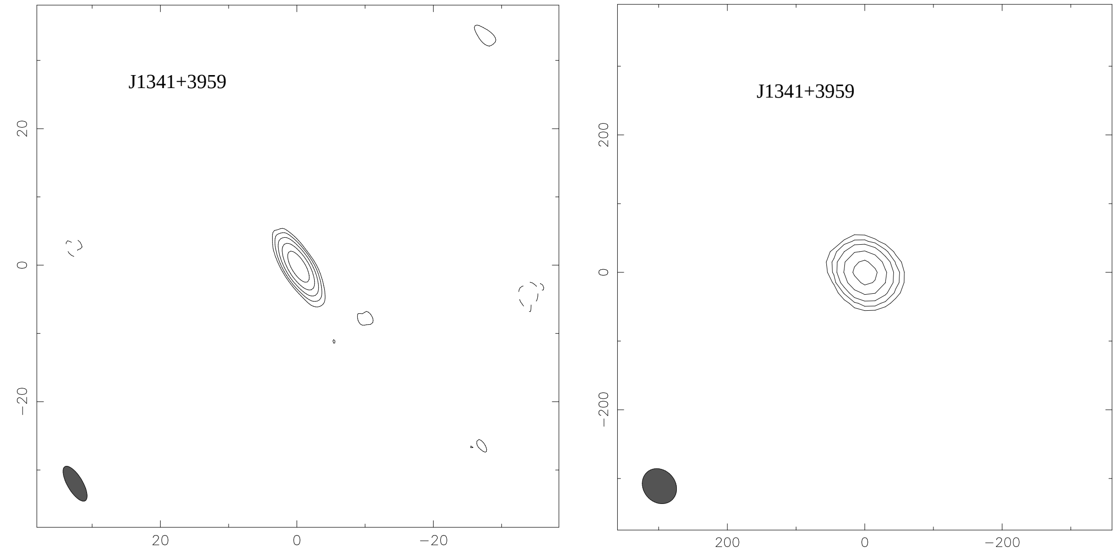

Figure 6. The EVN (left) and MERLIN (right) images of RXS J1341+3959 at 5 GHz. The contour levels are (-1, 1, 2, 4, 8, 16, 32, 64...) multiples the minimum contour level, which is 3 times the rms noise given in Table 2. The horizontal axis is the relative R. A., and the vertical axis is the relative Dec. to the source position in mas.

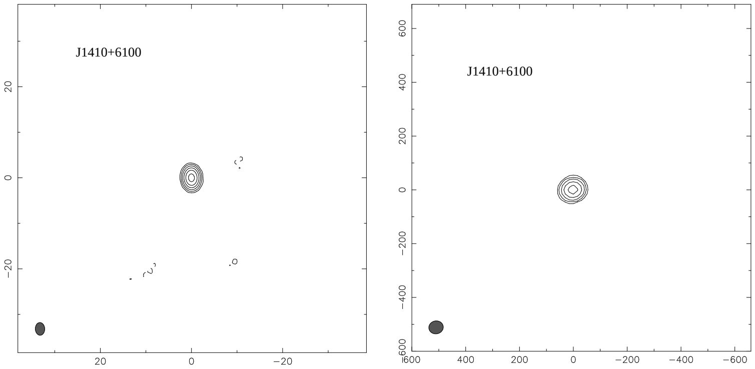

Figure 7. The EVN (left) and MERLIN (right) images of RXS J1410+6100 at 5 GHz. The contour levels are (-1, 1, 2, 4, 8, 16, 32, 64...) multiples the minimum contour level, which is 3 times the rms noise given in Table 2. The horizontal axis is the relative R. A., and the vertical axis is the relative Dec. to the source position in mas.

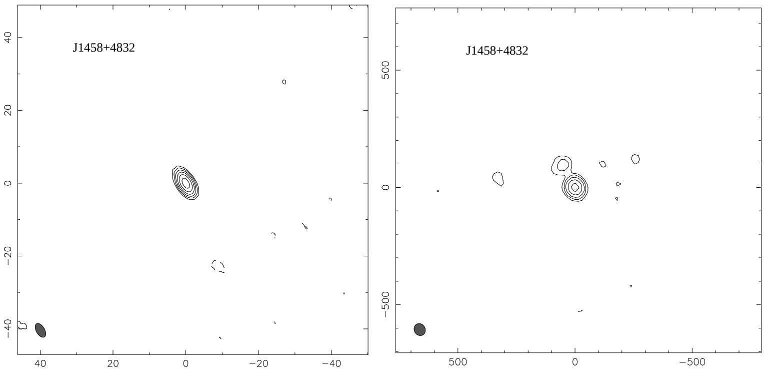

Figure 8. The EVN (left) and MERLIN (right) images of RXS J1458.4+4832 at 5 GHz. The contour levels are (-1, 1, 2, 4, 8, 16, 32, 64...) multiples the minimum contour level, which is 3 times the rms noise given in Table 2. The horizontal axis is the relative R. A., and the vertical axis is the relative Dec. to the source position in mas.

4 DISCUSSION

4.1 The brightness temperature

From the high-resolution VLBI images, the brightness temperature of radio core $T_{\rm B}$ in the rest frame can be estimated with (Ghisellini et al. 1993)

$$T_{\rm B}=\frac{S_\nu\lambda^2}{2k\Omega_{\rm s}}=1.77\times10^{12}(1+z)(\frac{S_\nu}{\rm Jy})(\frac{\nu}{\rm GHz})^{-2}(\frac{\theta_d}{\rm mas})^{-2} \quad (1)$$

in which z is source redshift, S_ν is core flux density at frequency ν, and $\theta_{\rm d}$ is source angular diameter $\theta_{\rm d}=a$ with a being the radius of circular components. The intrinsic brightness temperature $T_{B'}$ can be related with T_B by

$$T'_{\rm B}=T_{\rm B}/\delta. \quad (2)$$

Normally, the upper limit of physically realistic brightness temperature of nonthermal radio emission can be taken as the equipartition brightness temperature $T_{\rm in}=5\times10^{10}$ K (Readhead 1994).

We have calculated the brightness temperature in the source rest frame for the core components of these nine UHBLs (see Table 3), in which the measurements from the multi-epoch and multi-frequency VLBA archive data are also given. The distribution of all measured brightness temperature is shown in Fig. 10. The mean and median values of $T_{\rm b}$ for the radio core are $\sim 10^{11}$ K, which exceeds the equipartition brightness temperature $T_{\rm in}$. The high brightness temperature suggests that the beaming effect likely presents in all sources, and it can be quite strong in some sources, for example, $T_{\rm b}=10^{12.89}$ K in RXS J1458.4+4832, which is even greater than the inverse Compton catastrophic brightness temperature 10^{12} K (Kellermann & Pauliny-Toth 1969).

4.2 The Fermi γ-ray detection

The γ-ray emission of four sources are detected by the Fermi Large Area Telescope (LAT), and they are listed in the second AGNs catalog (Ackermann et al. 2011), i.e. 2E 0414+0057 with γ-ray photon index Γ=1.98, EXO 0706.1+5913 (Γ=1.28), RXS J1012+4229 (Γ=1.87), RXS J2304+3705 (Γ=1.96). The detection of γ-ray emission provide another evidence of beaming effect in these sources, in addition to the high brightness temperature. We note that their γ-ray photon index Γ are all smaller than 2.0. This indicates that the peak frequency of inverse compton scattering could be higher than the Fermi γ-ray frequency, which is consistent with their high synchrotron peak frequency. Indeed, the photon index are generally consistent with the mean photon index of HBLs 1.90 ± 0.17 (Ackermann et al. 2011), confirming their source classification.

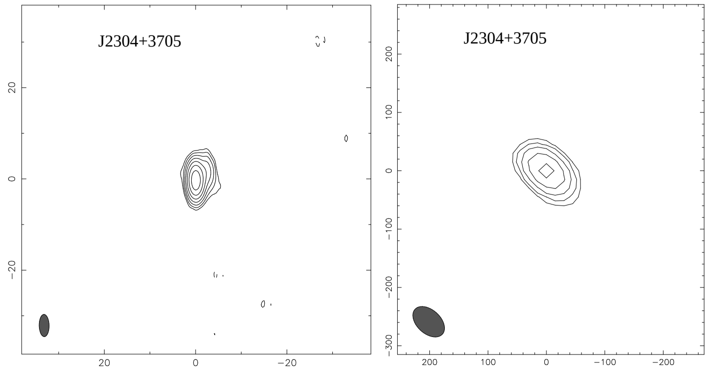

Figure 9. The EVN (left) and MERLIN (right) images of RXS J2304.6+3705 at 5 GHz. The contour levels are (-1, 1, 2, 4, 8, 16, 32, 64...) multiples the minimum contour level, which is 3 times the rms noise given in Table 2. The horizontal axis is the relative R. A., and the vertical axis is the relative Dec. to the source position in mas.

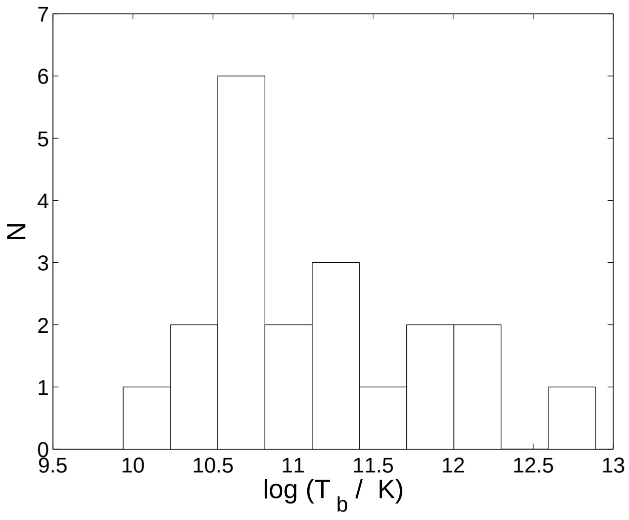

Figure 10. The histogram of brightness temperature of radio cores in all sources from our observations and all VLBA archive data.

All four sources are resolved with core-jet structure, while only one source has core-jet structure in the rest five non-Fermi detected sources. It thus seems that the Fermi detected BL Lac objects are more likely to have longer jets than non-Fermi sources in our sample. Although our sample is rather small, it is consistent with the results shown in Linford et al. (2011) that the short jet and point source BL Lacs are less likely to produce γ-rays. About 75% of the LAT BL Lacs are classified as long jets, compared to only 45% for the non-LAT BL Lacs.

4.3 The proper motion

In our nine sources, the proper motion can only be investigated for two sources 2E 0414+0057 and EXO 0706.1+5913. In 2E 0414+0057, the VLBI observations were collected at eight epochs covering about 14 years (see Table 1). Two jet components are detected and labeled as C1 and C2 (see Fig. 1). The relationship of their distance to the radio core with the observational time is plotted in Fig. 11. The weighted linear fits of each jet component were performed in order to calculate the proper motion, which is shown as solid lines in Fig. 11. The estimated proper motion are -0.02 ± 0.008 mas yr^{-1} and -0.038 ± 0.021 mas yr^{-1} for C1 and C2, respectively. We found that the C1 position at 8.4 GHz is consistent with that of 5 GHz, with a bit smaller distance to the core. Therefore, we tentatively combined position measurements at all frequency to estimate proper motion, however, this may cause uncertainties in estimating the proper motion, and can be part reason of negative proper motion. Our results can only be treated as indicative, not conclusive. But, at least, it shows that the proper motion is not large in 2E 0414+0057, and jet components are more like stationary.

In EXO 0706.1+5913, three jet components are identified as C1, C2 and C3 in our EVN image (see Fig.2). To investigate the jet proper motion, the VLBA archive data were collected at four epochs, with the measurements shown in Table 3. At epoch 2010.93, a new component C0' is found at a distance of 1.6 mas to core, which however is not detected in other observations. It may either be resolved due to the higher resolution at 8.6 GHz, or completely a new component. EXO 0706.1+5913 was observed at 1.6 GHz with EVN array at June 7, 2002 (Giroletti et al. 2006). The source was resolved to core and one jet component, which is identified as C3, according to its P.A. and distance to the core. From all available data, C1 was measured at three epochs, while only two epochs for C2 and C3 (see Table 3). The proper motion of C1, C2 and C3 are then estimated from multi-epoch data (Fig. 12), with values of 0.113 ± 0.115 mas yr^{-1} , 0.638mas yr^{-1} and 0.835mas yr^{-1}, corresponding to 0.93c, 5.24c and 6.87c for C1, C2 and C3, respectively. While C1 seems to have subluminal motion, the superluminal motion is only likely detected in C2 and C3, due to the fact that the proper motions of these two components are only estimated from two epochs.

4.4 The source compactness

Giroletti et al. (2004a) have used a ratio between the arcsecond core flux at 5 GHz $S^{''}$ and the correlated VLBI total flux at the same frequency $S_{\rm VLBI}$ to show that only a small fraction ($\sim$ 30%) of BL Lac objects has a complex subarcsecond structure invisible in their data. To investigate the compactness and compare with normal HBLs, we used the MERLIN flux as the lower limit of arcsecond core flux $S^{''}$, and EVN total flux for $S_{\rm VLBI}$ to calculate the ratio $S_{\rm VLBI}/S^{''}$ for our nine sources. The $S_{\rm VLBI}/S^{''}$ distributions for our sample is compared in Fig. 13 to that of the HBLs sample selected from Giroletti et al. (2004a). We found that our UHBLs sample has relatively lower values of $S_{\rm VLBI}/S^{''}$ than HBLs, with mean and median values of about 0.5 and 0.84, respectively. The result indicates that our UHBLs sources are less compact than the normal HBLs, likely due to the less beaming effect.

4.5 The flux variations

The multi-epoch VLBI observations of 2E 0414+0057 and EXO 0706.1+5913 are collected to explore the variations both in the core flux and total flux. The core and total flux density against the observation time are presented in Figs. 14 and 15. The significances of the variations were calculated using the method presented by DiPompeo et al. (2011),

$$\sigma_{\rm var} = \frac{|S_2 - S_1|}{\sqrt{\sigma_2^2 + \sigma_1^2}}$$

where S_1 and S_2 are flux at two epochs, and σ_1 and σ_2 are the corresponding flux uncertainties. We calculated $\sigma_{\rm var}$ with the fluxes at every two epochs at the same frequency. The largest $\sigma_{\rm var}$ of 2E 0414+0057 are 2.2 and 3.2 for the core and total flux, respectively, while 1.0 and 2.7 for EXO 0706.1+5913. All the values are smaller than the limit value of flux variations $\sigma_{\rm var} > 4$ given by DiPompeo et al. (2011). Therefore, there are no significant variations for both the core and total flux in these two sources, implying that the beaming effect are likely not severe.

4.6 UHBLs and HBLs

Our EVN observations show that the core-jet structure is clearly detected in five of nine sources. Albeit with a lower detection rate of jet structure, this is similar to the parsec-scale jet structure in HBLs and LBLs (Giroletti et al. 2004a; Kharb et al. 2008; Wu et al. 2007). No counter-jets are detected from our observations. All sources are unresolved with MERLIN, except for J1012+4229, J1319+1405 and J1458+4832, in which the signs of jet structure can be seen (see Figs. 1 - 9).

Normally, it is believed that there are many differences between LBLs and HBLs, including the multi-band luminosities (Nieppola et al. 2006), the redshift distribution (Kharb et al. 2008), the Doppler factors (Wu et al. 2007), and so on. Kharb et al. (2008) and Giroletti et al. (2004a) shows that the distribution of total radio power at 1.4 GHz for HBLs and LBLs are significantly different. However, the differences between LBLs, IBLs, HBLs and UHBLs are less discussed. To tackle this issue, we collected the data of redshfit, NVSS 1.4 GHz luminosity $L_{\rm NVSS}$ and 5 GHz luminosity $L_{5~\rm GHz}$ for the BL Lacs sample in Nieppola et al. (2006), in which each BL Lac object was classified individually. The differences of UHBLs with LBLs, IBLs, and HBLs are investigated with Kolmogorov-Smirnov (KS) test on the distribution of each parameter, and the results are shown in Table 5 in which the source numbers of each populations are also shown. We found that the UHBLs and HBLs have no significant difference in the distribution of $L_{\rm NVSS}$ and redshift, while different in $L_{5~\rm GHz}$. Since 1.4 GHz radio luminosities are likely less effected by the beaming effect, therefore, the similar distribution of HBLs and UHBLs indicates that these two populations may be intrinsically same (see also Wu et al. 2012). On the other hand, the different distribution of $L_{5~\rm GHz}$ implies that the beaming effect could be different, e.g. a less beaming effect in UHBLs, due to the fact that $L_{5~\rm GHz}$ are more influenced by the beaming effect. While the significant differences are found between UHBLs and LBLs, it's interesting to note that UHBLs are similar to IBLs according to the KS test results. Recently, Meyer et al. (2011) have argued that the IBLs are more misaligned versions of HBLs with similar jet powers. This scenario could also be appropriate for UHBLs, at least it is consistent with the results from direct comparison with HBLs.

Although the high brightness temperature and γ-ray detection imply that the beaming effect is likely presented in each UHBLs, the less compact radio structure, the less variations and proper motion (although only in several sources) all suggest that the beaming effect may not be strong, likely less than that of HBLs. Wu et al. (2007) found an strong anti-correlation between the Doppler factor and synchrotron peak frequency. Since UHBLs are at the high end of peak frequency distribution, they are expected to systematically have lower value of Doppler factor. Our results seem to be consistent with these expectations. A lower Doppler factor may indicate a larger viewing angle in UHBLs as expected from Wu et al. (2007). Alternatively, the Fermi γ-rays detections in four of nine sources imply that the jet velocity possibly has significantly decreased with respect to the very inner part, however with a small viewing angle generally required by the common large Doppler factors in γ-ray emission.

Our UHBLs are directly selected form Nieppola et al. (2006). However, the authors have argued that the actual position of the peak is probably exaggerated by the use of a parabolic fitting function, the peak frequencies of these objects cannot be considered as definite. One extreme possibility is that these sources are completely not real UHBLs. As shown in Abdo et al. (2010), no evidence was found for the

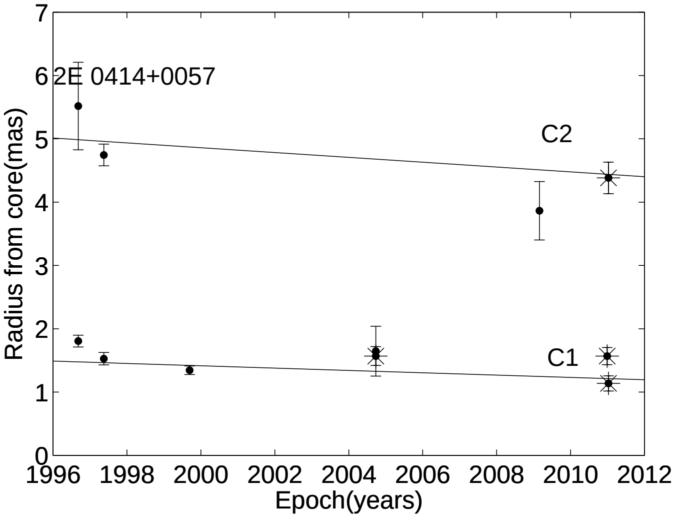

Figure 11. The jet proper motion of 2E 0414+0057. The weighted linear fits are shown as solid lines for C1 (lower) and C2 (upper). The solid circles are for data at 5 GHz, and the asterisks at 8 GHz (see text for details).

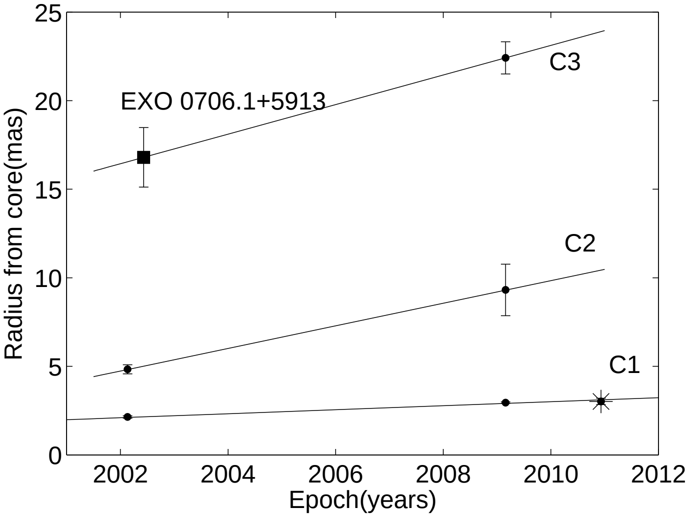

Figure 12. The jet proper motion of EXO 0706.1+5913. The weighted linear fits are shown as solid lines for C1, C2 and C3. The solid circles are for data at 5 GHz, and the asterisks at 8 GHz (see text for details), while the square stands for the 1.6 GHz data component from Giroletti et al.(2006).

hypothetical class of UHBLs characterized by a synchrotron emission that is so energetic to reach the γ-ray band. Although it is not definite, we can still see that $\nu_{\rm peak}$ of these sources are apparently higher than normal HBLs according to their SED in Nieppola et al. (2006). These points might be kept in the mind when further analyzing our results. The future simultaneous multi-band data analysis are necessary to explore their source nature, for example, by model-fitting with synchrotron and synchrotron self-compton.

5 SUMMARY

We present the EVN and MERLIN observations for nine UHBLs selected from Nieppola et al. (2006). The VLBA archive data are also combined to investigate their radio structure and properties. We found that the core-jet structure is detected in five sources, while four sources only have compact core on pc scale. The core of all sources show high brightness temperature (with mean and median values **log** ($T_{\rm b}$/K) $\sim$ 11, which implies that the beaming effect likely present in all sources. When multi-epoch VLBI data are available, we found no significant variations either for core or total flux density in two sources (2E 0414+0057 and EXO 0706.1+5913), and no evident proper motion is found in 2E

Table 3. Results of modelfit parameters.

Source	Epoch	Freqency (GHz)	Comp.	Flux density (mJy)	r (mas)	P.A.	a (mas)	log T_b (K)
2E 0414+0057	1996.68	4.99	C0	36.23 ± 3.66	0.00 ± 0.02	0.00	0.57 ± 0.04	10.25
	1996.68	4.99	C1	9.80 ± 2.06	1.81 ± 0.09	56.70	1.81 ± 0.19	
	1996.68	4.99	C2	1.85 ± 1.01	5.52 ± 0.69	104.26	2.84 ± 1.38	
	1997.38	4.99	C0	43.15 ± 4.11	0.00 ± 0.01	0.00	0.40 ± 0.03	10.79
	1997.38	4.99	C1	5.81 ± 1.79	1.53 ± 0.10	71.37	1.65 ± 0.20	
	1997.38	4.99	C2	2.78 ± 1.39	4.75 ± 0.17	124.09	2.30 ± 0.34	
	1999.70	4.99	C0	37.64 ± 4.86	0.00 ± 0.02	0.00	0.54 ± 0.05	10.33
	1999.70	4.99	C1	9.48 ± 2.78	1.35 ± 0.07	80.15	1.07 ± 0.13	
	2004.73	4.99	C0	38.82 ± 4.87	0.00 ± 0.02	0.00	0.39 ± 0.03	10.79
	2004.73	4.99	C1	7.73 ± 2.21	1.65 ± 0.39	73.29	3.90 ± 0.79	
	2004.73	8.42	C0	40.49 ± 4.63	0.00 ± 0.01	0.00	0.29 ± 0.02	10.75
	2004.73	8.42	C1	5.04 ± 1.72	1.57 ± 0.15	86.41	1.08 ± 0.30	
	2009.16	4.99	C0	45.57 ± 4.39	0.00 ± 0.01	0.00	0.33 ± 0.02	11.08
	2009.16	4.99	C2	8.64 ± 2.40	3.86 ± 0.46	90.68	3.56 ± 0.92	
	2010.99	8.65	C0	29.01 ± 2.36	0.00 ± 0.00	0.00	0.12 ± 0.01	11.73
	2010.99	8.65	C1	5.28 ± 1.16	1.57 ± 0.14	73.87	1.38 ± 0.27	
	2011.02	8.65	C0	35.27 ± 2.39	0.00 ± 0.01	0.00	0.27 ± 0.01	10.72
	2011.02	8.65	C1	9.97 ± 1.39	1.14 ± 0.12	81.33	1.98 ± 0.24	
	2011.02	8.65	C2	1.27 ± 0.51	4.38 ± 0.25	88.15	1.46 ± 0.50	
EXO 0706.1+5913	2002.13	5.00	C0	29.89 ± 3.56	0.00 ± 0.02	0.00	0.40 ± 0.04	10.56
	2002.13	5.00	C1	1.58 ± 0.87	2.14 ± 0.07	-128.91	0.40 ± 0.14	
	2002.13	5.00	C2	1.66 ± 0.93	4.83 ± 0.25	-156.42	1.11 ± 0.51	
	2004.73	4.99	C0	29.43 ± 5.00	0.00 ± 0.01	0.00	0.22 ± 0.03	11.32
	2004.73	8.42	C0	34.93 ± 5.90	0.00 ± 0.01	0.00	0.13 ± 0.02	11.70
	2009.16	4.99	C0	35.01 ± 2.16	0.00 ± 0.01	0.00	0.24 ± 0.01	11.32
	2009.16	4.99	C1	6.55 ± 0.94	2.95 ± 0.05	-147.26	0.87 ± 0.09	
	2009.16	4.99	C2	2.34 ± 1.16	9.31 ± 1.45	-156.27	5.92 ± 2.91	
	2009.16	4.99	C3	0.73 ± 0.49	22.42 ± 0.91	-145.37	2.83 ± 1.82	
	2010.93	8.65	C0	36.22 ± 2.89	0.00 ± 0.00	0.00	0.16 ± 0.01	11.41
	2010.93	8.65	C0’	1.80 ± 0.83	1.60 ± 0.01	-170.87	0.17 ± 0.03	
	2010.93	8.65	C1	3.54 ± 1.07	3.02 ± 0.18	-147.79	1.31 ± 0.36	
1ES 0927+500	2009.16	4.99	C0	12.59 ± 1.24	0.00 ± 0.01	0.00	0.28 ± 0.02	10.69
RXS J1012.7+4229	2009.16	4.99	C0	19.00 ± 1.42	0.00 ± 0.00	0.00	0.12 ± 0.01	11.99
	2009.16	4.99	C1	3.14 ± 0.67	3.47 ± 0.06	6.41	1.35 ± 0.12	
	2009.16	4.99	C2	2.62 ± 0.78	11.68 ± 0.81	25.21	5.63 ± 1.62	
RGB 1319+140	2009.16	4.99	C0	28.04 ± 2.30	0.00 ± 0.01	0.00	0.35 ± 0.02	10.85
	2009.16	4.99	C1	4.44 ± 1.12	5.83 ± 0.41	77.38	3.46 ± 0.81	
	2009.16	4.99	C2	0.81 ± 0.41	12.43 ± 0.19	80.49	1.07 ± 0.38	
RXS J1341+3959	2009.16	4.99	C0	6.71 ± 1.06	0.00 ± 0.00	0.00	0.08 ± 0.01	12.03
RXS J1410+6100	2009.16	4.99	C0	7.16 ± 0.90	0.00 ± 0.00	0.00	0.08 ± 0.01	12.06
RXS J1458.4+4832	2009.16	4.99	C0	7.64 ± 0.93	0.00 ± 0.00	0.00	0.05 ± 0.00	12.89
RXS J2304.6+3705	2009.16	4.99	C0	10.35 ± 0.95	0.00 ± 0.02	0.00	0.51 ± 0.03	9.94
	2009.16	4.99	C1	0.90 ± 0.29	3.01 ± 0.13	-59.25	1.15 ± 0.25	

Table 4. The VLBI positions of UHBLs.

Source	calibrator	R. A. (h m s) (J2000)	Dec. (d m s) (J2000)	R. A. (h m s) (J2000)	Dec. (d m s) (J2000)	data
1ES 0927+500	J0929+5013	09 30 37.574	+49 50 25.60	09 30 37.574	+49 50 25.549	EVN
RXS 1012.7+4339	J1022+4239	10 12 44.288	+42 29 57.010	10 12 44.305	+42 29 57.095	EVN
RGB 1319+140	J1327+1223	13 19 31.74	+14 05 33.140	13 19 31.742	+14 05 33.120	EVN
RXS J1341.0+3959	J1340+3754	13 41 04.920	+39 59 35.160	13 41 05.108	+39 59 45.420	MERLIN
RXS J1410.5+6100	J1400+6210	14 10 31.700	+61 00 10.000	14 10 30.851	+61 00 12.790	MERLIN
RXS J1458.4+4832	J1500+4751	14 58 27.353	+48 32 45.99	14 58 27.360	+48 32 45.979	EVN
RXS J2304.6+3705	J2301+3726	23 04 36.630	+37 05 07.3	23 04 36.715	+37 05 07.422	EVN

Column(1): Source name; Column(2): phase referencing calibrator; Columns (3) - (4): source position (R. A. and Dec.) from NED; Columns (5) - (6): source position (R. A. and Dec.) measured from our observations; Column (7) the data used to measure source position.

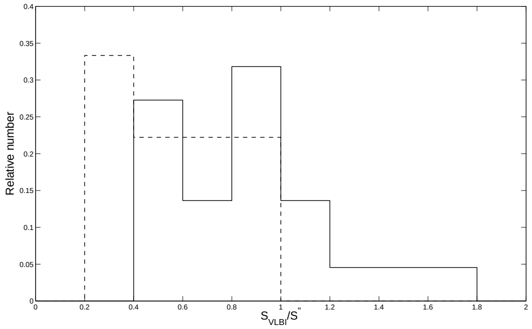

Figure 13. The distribution of $S_{\rm VLBI}/S^{''}$ for our UHBLs and HBLs of Giroletti et al. 2004a. The dashed line indicates the UHBLs, while the real solid lines indicates HBLs

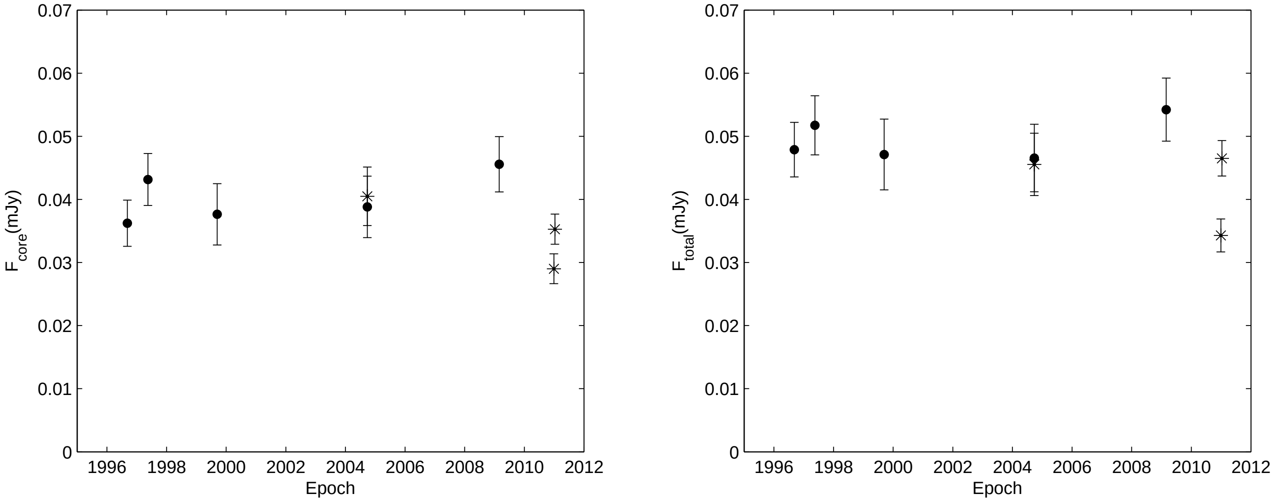

Figure 14. The flux variations in 2E 0414+0057: (left) the core flux, (right) the total flux. The solid circles and asterisks are for radio flux at 5 and 8 GHz, respectively.

0414+0057, while the superluminal motion is likely detected in EXO 0706.1+5913. Our sources are found to be less compact than the typical HBLs in Giroletti et al. (2004a), by comparing the ratio of the VLBI total flux to the core flux at arcsec scale. Combining all our results, we propose that the beaming effect might be present in the jets of UHBLs, however, it is likely weaker than that of typical HBLs. Moreover, UHBLs could be the less Doppler beamed versions of HBLs with similar jet power. The results are in good consistence with the expectations from our previous work.

ACKNOWLEDGMENTS

We thank the anonymous referee for insightful comments and constructive suggestions. This work is supported by the NSFC grants (No. 10978009, 11163002, 10833002, 11073039, and 10803015), and by the 973 Program (No. 2009CB824800). The European VLBI Network is a joint facility of European, Chinese, and other radio astronomy institutes funded by their national research councils. The National Radio Astronomy Observatory is operated by Associated Universities, Inc., under cooperative agreement with the National Science Foundation. MERLIN is a National Facility operated by the University of Manchester at Jodrell Bank Observatory on behalf of PPARC. This research has made use of NASA/IPAC Extragalactic Database (NED), which is operated by the Jet Propulsion Laboratory, California Institute of Technology, under contract with National Aeronautics and Space Administration.

REFERENCES

Abdo, A. A., Ackermann, M., Agudo, I., et al. 2010, ApJ, 716, 30
Ackermann, M., Ajello, M., Allafort, A., et al. 2011, ApJ, 743, 171
Becker R. H., White R. L., Helfand D. J., 1995, ApJ, 450, 559
Chen, Y. J., Zhang, F. J., Sjouwerman, L. O. 1999, Ap&SS, 266, 495

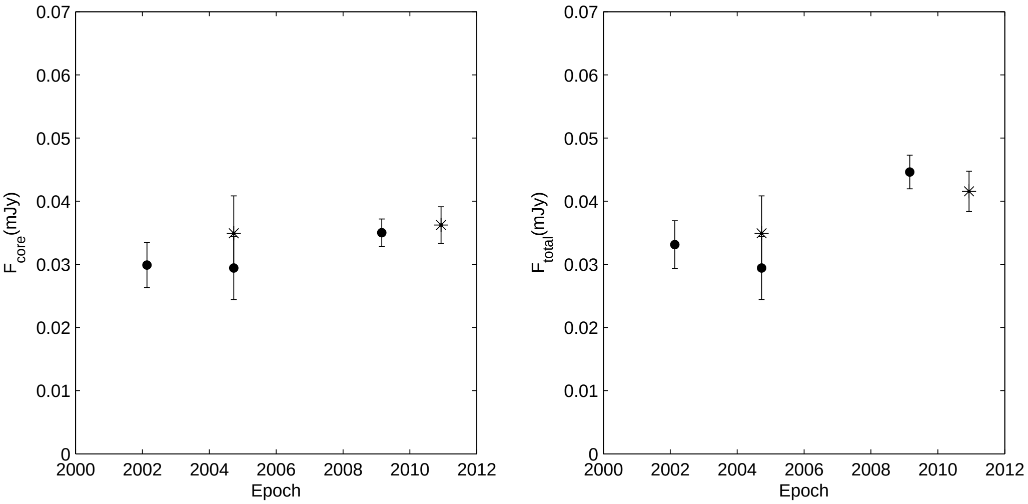

Figure 15. The flux variations in EXO 0706.1+5913: (left) the core flux, (right) the total flux. The solid circles and asterisks are for radio flux at 5 and 8 GHz, respectively.

Table 5. The KS test on UHBLs with HBLs, IBLs and LBLs.

Parameter	KS statistic	probability	Significantly different	subsets	$N_{subsets}$	N_{UHBLs}
$L_{\rm NVSS}$	0.305	0.127	NO	HBLs	71	17
	0.265	0.253	NO	IBLs	68	...
	0.651	7.2328e-06	YES	LBLs	69	...
z	0.258	0.228	NO	HBLs	74	19
	0.194	0.574	NO	IBLs	73	...
	0.3158	0.0763	YES	LBLs	76	...
$L_{5\ \rm GHz}$	0.3673	0.08	YES	HBLs	49	14
	0.2653	0.3708	NO	IBLs	49	...
	0.7255	6.3715e-06	YES	LBLs	51	...

Fossati, G., Maraschi, L., Celotti, A., Comastri, A., & Ghisellini, G. 1998, MNRAS, 299, 433
Gabuzda, D. C., Pushkarev, A. B., Cawthorne, T. V., 2000, MNRAS, 319, 1109
Ghisellini, G. 1999, ApL&C, 39, 17
Giommi, P., Ghisellini, G., Padovani, P., & Tagliaferri, G. 2001, AIPC, 599, 441
Giroletti, M., Giovannini, G., Taylor, G. B., & Falomo, R. 2004a, ApJ, 613, 752
Giroletti, M., Giovannini, G., Feretti, L., et al. 2004b, ApJ, 600, 127
Giroletti, M., Giovannini, G., Taylor, G. B., Falomo, R. 2006, ApJ, 646, 801
Ghisellini G., Padovani P., Celotti A., Marasch L., 1993, ApJ, 407, 65
Ghisellini, G., Celotti, A., Fossati, G., Maraschi, L. & Comastri, A. 1998, MNRAS, 301, 451
Jorstad, S. G., Marscher, A. P., Mattox, J. R., et al. 2001, ApJ, 556, 738
Kellermann, K. I., & Pauliny-Toth, I. I. K. 1969, ApJ, 155, L71
Kharb, P., Gabuzda, D., Shastri, P. et al. 2008, MNRAS, 384, 230
Linford, J. D., Taylor, G. B., Romani, R., et al. 2011, ApJ, 726, 16
Meyer, E. T., Fossati, G., Georganopoulos, M., et al. 2011, ApJ, 740, 98 1107.5105
Nieppola, E., Valtaoja, E., Tornikoski, M., Hovatta, T., Kotiranta, M. 2008, A&A, 488, 867
Nieppola, E., Tornikoski, M., & Valtaoja, E. 2006, A&A, 445, 441
Padovani, P., & Giommi, P. 1995, ApJ, 446, 547
Padovani, P., 2007, AP&SS, 309, 63
Piner, B. G., & Edwards, P. G. 2004, ApJ, 600, 115
Piner, B. Glenn., Pant, Niraj., Edwards, Philip G., ApJ, 678, 64P
Rani, Bindu; Gupta, Alok C.; Bachev, R.; Strigachev, A.; Semkov, E.; et al. 2011, arXiv:1107.0597v1
Readhead A.C.S., 1994, ApJ, 426, 51
Rector, T. A., Gabuzda, D. C., & Stocke, J. T. 2003, AJ, 125, 1060
Wu, Z. Z., Jiang, D., R., Gu, M. F., Liu, Y., 2007, A&A, 466, 63
Wu, Z. Z., Gu, M. F., Jiang, D., R., 2009, RAA, 9, 168
Wu, Z. Z., Gu, M. F., Jiang, D., R., 2012, submit to APRIM